Thirteenth European Rotorcraft Forum

2.11

Paper No. 34

A VORTEX EMBEDDING METHOD FOR FREE WAKE ANALYSIS OF HELICOPTER ROTOR BLADES IN HOVER

John Steinhoff
K. Ramachandran

The University of Tennessee Space Institute
Tullahoma, Tennessee
USA

September 8-11, 1987

ARLES, FRANCE

A VORTEX EMBEDDING METHOD FOR FREE WAKE ANALYSIS OF HELICOPTER ROTOR BLADES IN HOVER

J. Steinhoff and K. Ramachandran

The University of Tennessee Space Institute
Tullahoma, Tennessee
USA

ABSTRACT

A method is described to compute flow over helicopter rotor blades. The method utilizes a compressible potential flow field with embedded vortex sheets. It is fully compressible, with the ability to capture shocks in transonic cases, and is able to treat the wake as free with no external inputs. Also, the wake is treated in a general, unified way as a surface that moves through the flow field with no constraints imposed by the computation.

The method is quite different from others being developed. In other approaches the wake is typically treated as a collection of separate filaments. Also, other compressible approaches typically break the computational region into a set of small regions near each blade where the compressible flow equations are solved, and an outer region where the wake is computed. These approaches do not appear to be adequate for modern rotor blades because the physical wake from each blade usually does not break up into a set of well-defined vortex filaments, and also because it can approach quite close to other blades.

The vortex embedding technique has been implemented in a computer code, **HELIX I**. In validation studies involving comparisons between results computed with **HELIX I** and experiments there has been very good agreement for the prediction of pressure distributions on blade surfaces, even in transonic cases with significant shocks. Also, the rotor wake geometry was also well predicted, for both two and four blade rotors. Successful prediction of the initial tip vortex descent rate (k_1) is especially notable because previous methods have difficulty doing so.

1. Introduction

Most current methods for computing rotor flow fields are based on integral or finite difference techniques[1]. Integral methods, in the form of lifting line or lifting surface methods are able to treat the rotor blade as well as the wake in a single unified way[2]. They, however, have several disadvantages; They are restricted to linear, low speed shock-free cases; They have difficulty attaining stable solutions, particularly in hover, where a large number of interacting vortex sheets must be treated; And, finally, the computation time increases rapidly with the number of elements used to represent the blade/vortex system (as the square of the number of elements). The most serious limitation is the low speed restriction, since modern rotor blades operate in the transonic regime, where compressibility is important, and shocks can exist in the flow.

Finite difference methods (also finite volume and finite element), on the other hand, usually can treat compressibility effects and can accurately solve for the flow in the immediate region of the blade. Most of these methods, which include Potential Flow and Euler based methods, however, do not treat the flow field in a single unified way: they isolate the region close to each blade and only solve the difference equations in those regions. The entire vortex system is currently treated in these methods by coupling with an integral technique, such as a classical lifting line or lifting surface method. This vortex calculation is used to determine an induced velocity on the surface of the finite difference grid surrounding each blade, which is then used as a boundary condition for the finite difference calculation in a coupled iteration scheme.

A unique exception to the above approaches is the technique that we have developed. This method, like the above finite difference ones, is fully compressible and can resolve transonic effects such as shocks. Unlike these others, however, it treats the entire relevant flow region, including the blades and vortex sheets, in a unified way. This entire region is discretized, and only far-field boundary conditions are used at the (distant) computational boundaries. In this way, solutions can be developed without concern as to whether the computed vortex sheet lies outside of a special artificial region about each blade.

Conventional Euler equation schemes are not suitable for such a unified approach because they attempt to solve for the internal structure of the sheet, as well as its motion. With Euler methods, accurate computation of a concentrated vortex sheet is only effective very close to the blade since numerical viscosity rapidly spreads the sheet as it is convected. This has lead some researchers to state that conventional Euler methods cannot be used for solving the rotor flow problem in a unified way, given currently available supercomputers[3]. Our approach differs from these, however, in that it permits modeling of the vorticity structure - and hence elimination of such artificial diffusion problems.

Also, a reason that such a unified approach is not feasible with conventional Potential methods is that they treat the vortex sheets as discontinuities in the Potential. Such a treatment constrains the sheets to lie on segments of surfaces of the computational grid.

Accordingly, in conventional Potential methods, only short segments of the sheets, which are fairly flat, and where the grid can be distorted to follow the sheet, can be accurately treated. This results, as in Euler methods, in a restriction to small regions near each blade[4].

We avoid the above problems by the use of an embedding procedure which allows us to put vorticity layers anywhere in the grid. Our method is based on the fact that any flow field can be decomposed into potential and vortical parts. A potential is defined on a set of grid points, as in standard methods. Also, as in these methods, the mass balance relations are enforced at each point on the grid. The potential, however, does not have any discontinuities, and therefore does not represent any vorticity. The vorticity is represented by a separate velocity field which is added to the gradient of the potential. The location and strength of this added field is determined by momentum considerations. This added field is concentrated in sheets, as is the vorticity that results from it. No external specification of the strength of these sheets or their location is required: momentum conservation relations are used to determine these, together with the mass balance relations. Thus, it is a true free-wake vortex method. The internal structure of the sheet can be modeled rather than resolved by the grid. Since this structure is determined by turbulent viscous effects and is of a smaller length scale than the other features of the problem, it is very economical to use such an approach. Conversely, to accurately resolve this thin, internal region with a finite difference scheme as it convects through the flow would be very costly. Some technical details concerning the embedding method are explained below and in Refs. (5) and (6).

2. Vortex Embedding Method

The basis of the Vortex Embedding procedure is in the fact that any velocity $\vec{q}$ can be expressed as the sum of a potential and vortical components:

$$\vec{q} = \vec{\nabla}\phi + \vec{q}^{v},$$
$$\vec{\omega} = \vec{\nabla} \times \vec{q}^{v}.$$

This decomposition is made especially powerful by the fact that for a given $\vec{\omega}$ distribution, $\vec{q}^{v}$ is not unique. This can produce some very useful simplifications. In a conventional full potential computations for the lifting flow about a wing, the entire velocity is usually represented by the potential, ϕ (that is $\vec{q}^{v} = 0$). However, the production of lift implies the shedding of circulation. With a potential alone this can only be represented by a sheet along which ϕ is discontinuous and where the magnitude of this discontinuity, Γ, is the shed circulation. This sheet requires special coding logic and typically must lie along a grid coordinate. However, the use of our velocity decomposition allows a considerable simplification and versatility in the sheet description. The basic idea is to spread the sheet into a thin vorticity region described by an appropriate velocity distribution, $\vec{q}^{v}$. This added velocity can take many forms, two of which are shown in Figs. 1 and 2.

The representation of Figure 1 shows a tangential velocity discontinuity being replaced by a region of spread tangential velocity variation. While this is a good picture of total velocity, $\vec{q}$, it would be a bad choice for $\vec{q}^v$. This is due to the fact that such a tangential $\vec{q}^v$ must extend throughout the entire flow field, even though the $\vec{\omega}$ field is nonzero in only a small region. This $\vec{q}^v$ field (which defines $\vec{\omega}$) is not small and requires a large amount of memory.

Another, more computationally efficient approach is to use a distribution of spread velocity normal to the sheet surface as shown in Figure 2. This representation seems very unphysical until one considers that it is not the entire velocity which is represented, but merely the vortical portion, $\vec{q}^v$. The total velocity, $\vec{q}$ must still be of the form shown in Figure 1, after the potential portion, $\vec{\nabla}\phi$, is added. The vortical part, $\vec{q}^v$, can have any form as long as $\vec{\omega} = \vec{\nabla} \times \vec{q}^v$. The normal form depicted in Figure 2 has the advantage of being nonzero only in a thin region, just like $\vec{\omega}$.

In order to find the required strength of $\vec{q}^v$ we use Gauss' theorem to obtain a relation for the integral of $\vec{q}^v$ along a normal through each point on the sheet;

$$\int q_n^v dn = \Gamma$$

The circulation, Γ, is known at the upstream edge of the sheet (blade trailing edge) from the lift distribution (which is computed as part of the entire calculation). Since it is constant along mean streamlines within the sheet it can easily be computed on the entire sheet. This relation provides a scaling factor which gives the magnitude of $\vec{q}^v$ as soon as the width of the layer and the functional form of ω is determined. This width and functional form can be found by using a viscous solution or by simply choosing computationally convenient values. For the rotor wake problem, the latter approach suffices.

The advantage of this type of representation is twofold:

1. It allows us to give a structure to the vorticity field $\vec{\omega}$. This field can be either solved for or modeled.

2. It allows us to put vorticity anywhere in the field with no constraints imposed by the grid. This frees us to convect vorticity quite easily.

With these features available to us we have constructed a combined Eulerian-Lagrangian code, "**HELIX I**", for the hover problem. In this code we solve the mass conservation equation $\vec{q}_\infty$

$$\vec{\nabla} \cdot (\rho \vec{q}) = 0, \tag{1}$$

$$\vec{q} = \vec{\nabla}\phi + \vec{q}^v + \vec{q}_\infty \tag{2}$$

where $\vec{q}_\infty$ is an irrotational field describing undisturbed flow and $\vec{q}^{\,v}$ is a normal velocity distribution describing a thin shed vorticity sheet which we allow to convect freely through the flow field. With this representation, $\vec{q}^v$ is a continuous vortical velocity field which suffers no artificial numerical diffusion.

For the hover problem it has sufficed to model $\vec{q}^v$ using functions which were chosen on the basis of numerical convenience alone. We can, however, include more accurate models of the vortex internal structure. This vorticity embedding thus gives our finite difference code the ability to predict more than the hovering blade transonic flow. It permits accurate wake descriptions and, further, the inclusion of flow features for which we have engineering models (whether or not analytical/computational approaches are available). Thus it provides a framework for an entire rotor flow calculation.

A particularly simple and accurate form for $\vec{q}^v$ involves a Clebsh-type of representation:

$$\vec{q}^v = \Gamma^c \vec{\nabla}\psi,$$

where $\Gamma^c(\vec{r})$ is a three dimensional field which smoothly goes to the appropriate Γ (circulation value) on the sheet as $\vec{r}$ approaches the sheet surface. The potential, $\psi(\vec{r})$, smoothly goes from + 1/2 on one side of the sheet to - 1/2 on the other. A convenient formula for $\psi(\vec{r})$ is

$$\begin{aligned}
\psi(\vec{r}) &= \frac{1}{2}\, sin\ (\pi S_n), |S_n| < a/2 \\
\psi(\vec{r}) &= +1/2 \quad , S_n > +a/2 \\
\psi(\vec{r}) &= -1/2 \quad , S_n < -a/2
\end{aligned}$$

where S_n is a (signed) normal distance from the point $\vec{r}$ to the sheet.

We use interpolation-like formulae to compute $\Gamma^c(\vec{r})$ and $S_n(\vec{r})$ at any grid point $\vec{r}$;

$$\begin{aligned}
\Gamma^c(\vec{r}) &= [\sum_\ell \Gamma_\ell \sigma(\Delta\vec{r}_\ell)]/A \\
\vec{S}_n(\vec{r}) &= [\sum_\ell \vec{S}^n_\ell(\vec{r},\vec{r}_\ell)\sigma(\Delta\vec{r}_\ell)]/A \\
S_n(\vec{r}) &= |\vec{S}_n(\vec{r})| \\
A &= \sum_\ell \sigma(\Delta\vec{r}_\ell), \\
\Delta\vec{r}_\ell &= \vec{r} - \vec{r}_\ell
\end{aligned}$$

where the Γ_l is the circulation defined for each marker, l, that defines the sheet. It remains constant on each marker from the point on the blade trailing edge where it is shed. Also, $\vec{S}^n_\ell(\vec{r},\vec{r}_\ell)$ is the normal distance from $\vec{r}$ to a plane through the sheet at marker ℓ, and the spreading function, $\sigma(\Delta\vec{r}_\ell)$ is

$$\sigma(\Delta\vec{r}_\ell) = max(0, 1 - \frac{\Delta\vec{r}_\ell^{\,2}}{a^2})$$

where a is a specified spreading distance.

Even through ψ is non-zero throughout the field (except on the sheet), $\vec{\nabla}\psi$ is zero beyond the spreading distance from the sheet. Accordingly, both $\Gamma^c(\vec{r})$ and $\psi(\vec{r})$ need be computed only on those grid points that are in a narrow band about the sheet with thickness of the order of the spreading distance. Another very important property of this $\vec{q}^v$ is, the elimination of spurious numerical vorticity in regions near the sheet where Γ is constant (no physical vorticity on the sheet). In such regions $\Gamma^c(\vec{r})$ will be constant and $\vec{q}^v$ can be written

$$\vec{q}^v = \vec{\nabla}(\Gamma^c \psi(\vec{r})).$$

Even though $\vec{q}^v$ is still non-zero, if the same numerical differencing scheme is used for $\vec{\nabla}\psi$ as is used for $\vec{\nabla}\phi$, the effect of the sheet in regions of zero vorticity will be identically zero. This was not true for our earlier formulation of $\vec{q}^v$, and resulted in a requirement for larger spreading distances and thicker vortices(for a given grid).

3. Solution Procedure

The calculations presented in Reference 7 were done with an initial formulation of the vortex embedding method. A new formulation has been developed based on the above Clebsch type decomposition for the vortical velocity calculation. This allows us to use a smaller vortex cross-section for a given grid, than the initial formulation. It can be shown that, as the grid is refined, the vortex spreading with the initial formulation must decrease less rapidly than the cell size. Otherwise numerical effects appear which can be reflected in the motion of the vortex. The new formulation allows us to embed a tight vortex sheet with small spreading, even in a fairly coarse, computationally efficient mesh.

We first decompose the velocity into a free stream, potential and vortical part:

$$\vec{q} = \vec{\Omega} \times \vec{r} + \vec{\nabla}\phi + \vec{q}^v \tag{1}$$

The vortical part, $\vec{q}^v$, is concentrated near the sheet as discussed in section 2. A fixed grid (in the rotating blade fixed frame) is used to solve the potential flow equation for the potential, ϕ:

$$\vec{\nabla} \cdot (\rho\vec{q}) = 0 \tag{2}$$

where ρ is the density given by

$$\rho = [1 - \frac{\gamma - 1}{2} M_\infty^2 \left((\vec{\Omega} \times \vec{r})^2 - \vec{q}^2 \right)^{\frac{1}{\gamma-1}}] \tag{3}$$

During iteration towards convergence (the solution is steady in the blade coordinate system for hover) a four step procedure is repeatedly used:

1) The vortex sheet position is integrated as a set of marker streamlines to follow the flow using interpolated values of $\vec{q}$ from the fixed grid

2) $\vec{q}^v$ is computed at grid points near the sheet

3) a potential, ϕ, is computed at grid points based on equation (2) using a modified finite volume potential flow technique.

4) A new velocity, $\vec{q}$, is computed at each grid point based on equation (1).

At convergence Equation (2) is satisfied and the vortex sheet follows the flow. Vorticity contours for a typical vortex sheet, computed with our new method, for a four bladed rotor that has gone around the rotor axis about 200 degrees are displayed in Fig. 3 in a cross-flow plane.

4. Results

In Figs. 4 – 6 computed results are presented for a two-blade rotor with an aspect ratio of 6.0, constant NACA0012 cross section, no twist, pitch of 8° and a tip Mach number of 0.436. These conditions match the experimental ones published in Ref. (8). In Fig. 4 the computed bound circulation is presented. In Figs. 5 and 6 the computed vertical motion and contraction of the tip vortex (calculated as the centroid of the computed vortex sheet) are presented, and compared with experimental results of Ref. (8). The comparison is seen to be fairly close, even though no adjustable parameters were used in the calculation. The slope of the vortex descent curve in Fig. 5 is close to the experimentally measured slope before the first blade crossing at 180^0. Also, the computed slope closely matches experiment near the second crossing at 360^0. The computed descent curve changes slope more gradually than experiment in the intermediate region. This is apparently due to the relatively large spreading used in the calculation, which results in overlap of the first and second vortices in this region.

In Figs. 7 – 13 results are presented for the same rotor with transonic tip Mach number of .877. The computed bound circulation is presented in Fig. 7, vortex vertical motion in Fig. 8 and contraction in Fig. 9. In Figs. 10 – 13 computed C_p values are presented and compared with experimental data for r/R values of .68, .80, .89 and .96, respectively. The comparison can be seen to be good except in the .96 case, which is very close to the tip. To resolve this region a finer grid is required there. Also, the relatively coarse grid used near the tip results in a vortex width there which is larger than experiment (although this width does not increase as the vortex convects). This can be seen in Figs. 6 and 9 where the vortex centroid does not start at the tip of the rotor, but slightly inboard.

The two-blade rotor results presented were done with an initial formulation of the vortex embedding method. Results for four-blade rotors were obtained using the new formulation.

One four-blade case computed involved a NACA0012 profile with an aspect ratio of 18.2, -8^0 linear twist, pitch at .75 span equal to 8^0 and tip Mach number .46. This corresponded to an experiment described in Ref. (9). The computed tip vortex descent is presented in Fig. 14 and the contraction in Fig. 15. Also, in Fig. 14 the two experimentally measured slopes, k_1 and k_2, for the descent before and after first blade passage are represented. The experimentally measured vortex radii are presented in Fig. 15. Agreement with experiment is seen to be very good.

Another four-blade case treated with the new formulation involved blade No. 7 of Ref. (10). It had an aspect ratio of 15, tip Mach number of .40, OA209 profile, pitch at .75 span (Θ_{75}) equal to 10^0, and linear twist such that pitch increased by 8.3^0 from root to tip. The computed circulation is compared in Fig. 16 to the experimental data of Ref. (10). The computed vortex geometry is plotted in Figs. 17 (height) and 18 (radial contraction) as a function of azimuthal angle and compared with experimental measurements of Ref. (10). Agreement between experimental and computed circulation as well as vortex geometry can be seen to be very good.

5. Conclusion

In conclusion, a vortex embedding method has been described for computing compressible free wake rotor flow fields in hover. The wake is treated as a continuous sheet and not approximated by discrete vortex filaments. Also, the wake is treated in a unified way with no assumptions as to how close it approaches other blades and without breaking the computational region into separate sub-grids near the blades.

The method, implemented in a code, **HELIX I**, was tested by computing a number of hover cases and comparing with experimental data. Good agreement with experiment was obtained in surface pressures and wake geometry for both subsonic and transonic cases (with significant shocks), and for both two and four bladed rotors. A new formulation, based on Clebsch-type potentials, was seen to be important for obtaining accurate wake geometries, in the regions where the wake from each blade passes close to the other blades.

5. References

1. W. Johnson, "Recent Developments in Rotory-Wing Aerodynamics," AIAA Journal, Vol.24, August, 1986.

2. J. D. Kocurek and J. L. Tangler, "A prescribed Wake Lifting Surface Hover Performance Analysis," 32nd Annual National Forum of the American Helicopter Society, May, 1976.

3. R. Aggarwal and J. Deese, " Euler Calculations for Flowfield of a Helicopter Rotor in Hover," presented at AIAA 4th Applied Aerodynamics Conference, San Diego, CA, June, 1986.

4. T. A. Egolf and S. P. Sparks, "Hovering Rotor Airload Prediction Using a Full Potential Flow Analysis with Realistic Wake Geometry," presented at the 41st Annual Forum of the American Helicopter Society, Ft. Worth, Texas, May, 1985.

5. J. Steinhoff, K. Ramachandran and K. Suryanarayana, "The Treatment of Convected Vortices in Compressible Potential Flow." AGARD Symposium on Aerodynamics of Vortical Type Flows in Three Dimensions," pg. 22-1, (AGARD-CPP-342) Rotterdam, Netherlands, April, 1983.

6. J. Steinhoff and K. Suryanarayana, "The Treatment of Vortex Sheets in Compressible Potential Flow," Page 1, Proceedings, AIAA Symposium on Computational Fluid Dynamics, Danvers, MA, July, 1983.

7. J. Steinhoff and K. Ramachandran, "Free Wake Analysis of Compressible Rotor Flow Fields in Hover," Paper No. 20, Twelfth European Rotorcraft Forum, Garmisch-Partenkirchen, Federal Republic of Germany, September, 1986.

8. F. X., Caradonna and C. Tung, "Experimental and Analytical Studies of a Model Helicopter Rotor in Hover, " NASA-TM-81232, 1981.

9. A. J. Landgrebe, "An Analytical and Experimental Investigation of Helicopter Rotor Hover Performance and Wake Geometry Characteristics," USAAMRDL Technical Report 71-24, June 1971.

10. C. Maresca, D. Favier and M. Nsi Mba, "A Prescribed Radial Circulation Distribution of a Hovering Rotor Blade," Paper No.23, Twelfth European Rotorcraft Forum, Garmisch-Partenkirchen, Federal Republic of Germany, September, 1986.

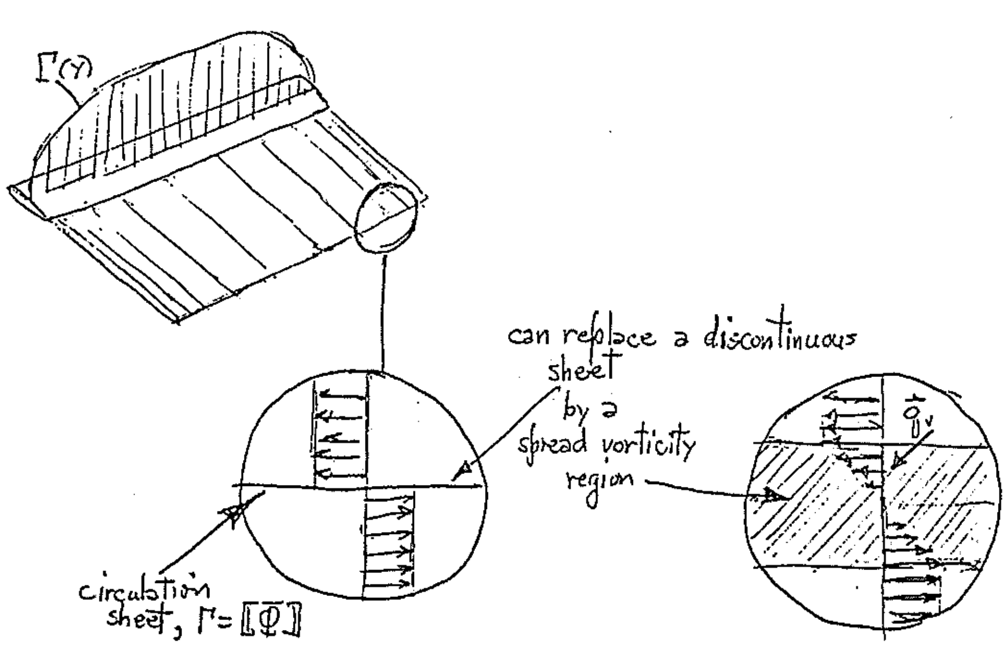

Figure 1.

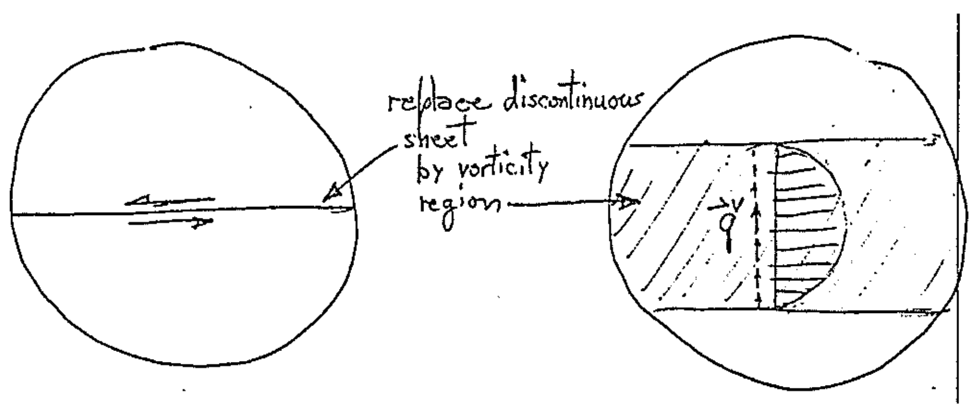

Figure 2.

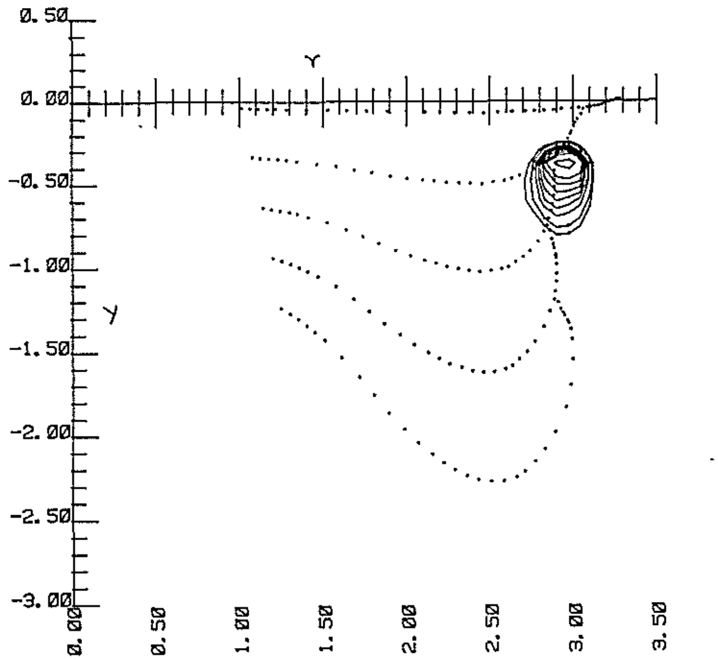

Figure 3.

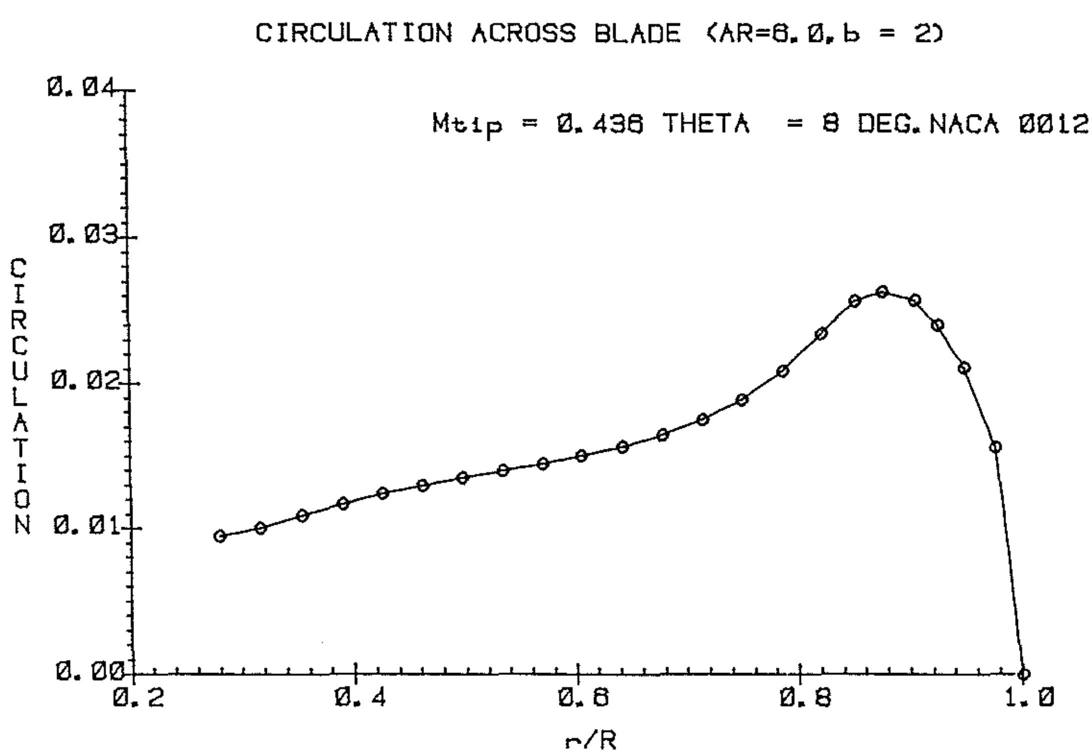

Figure 4.

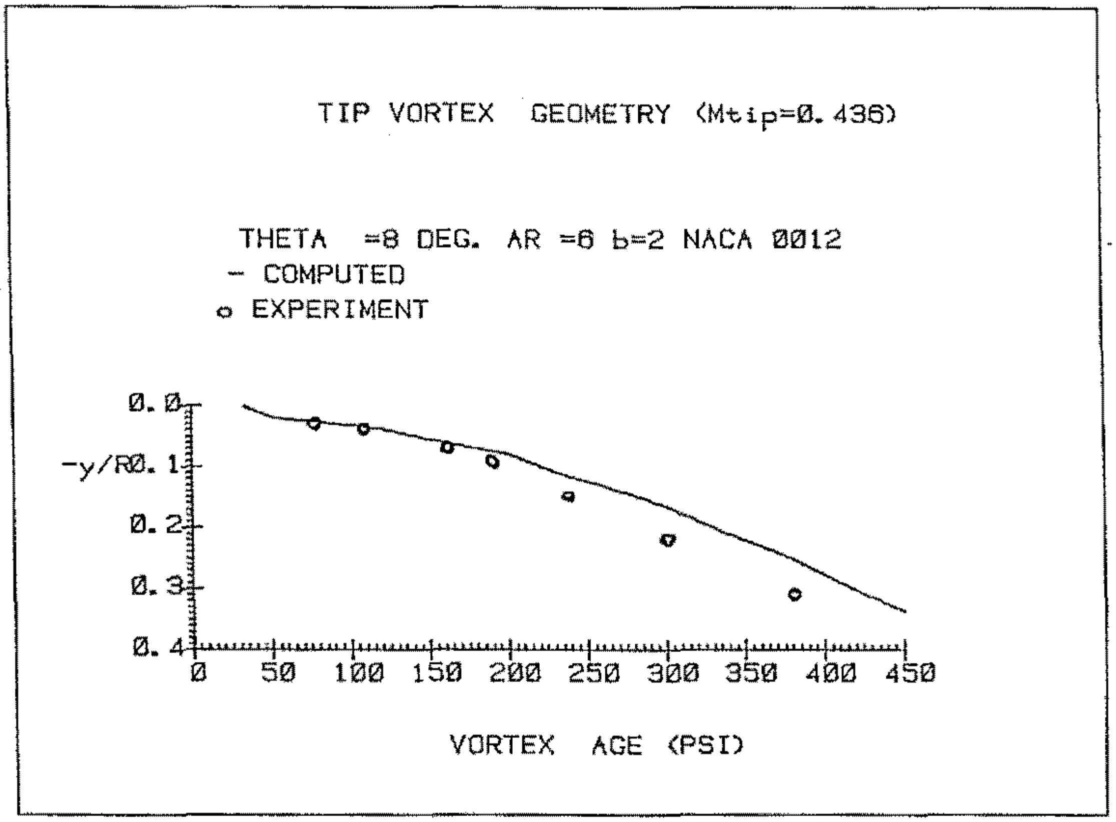

Figure 5.

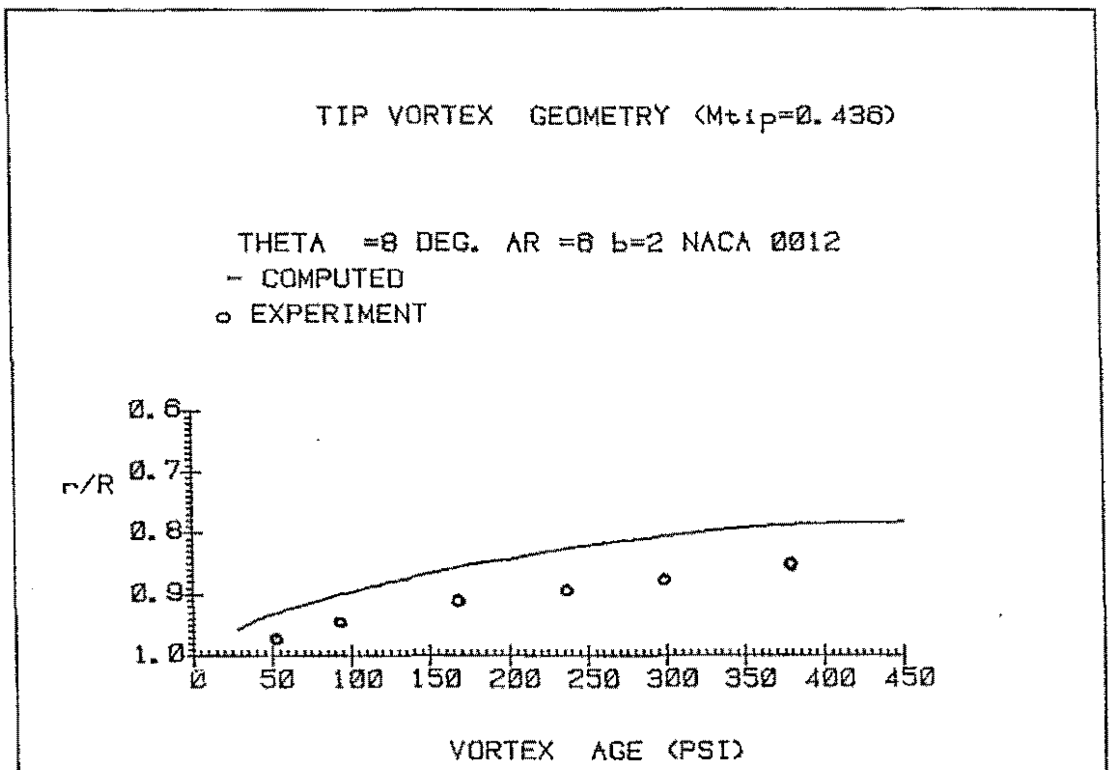

Figure 6.

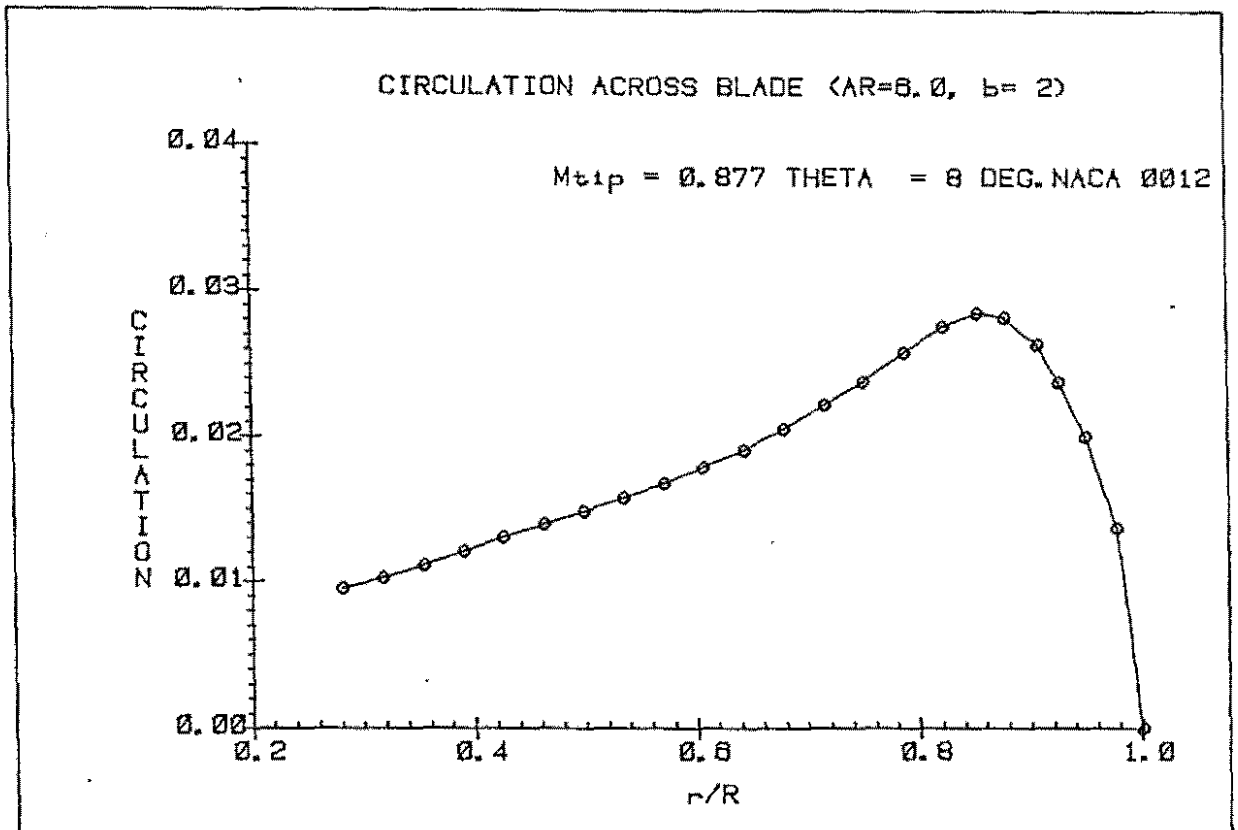

Figure 7.

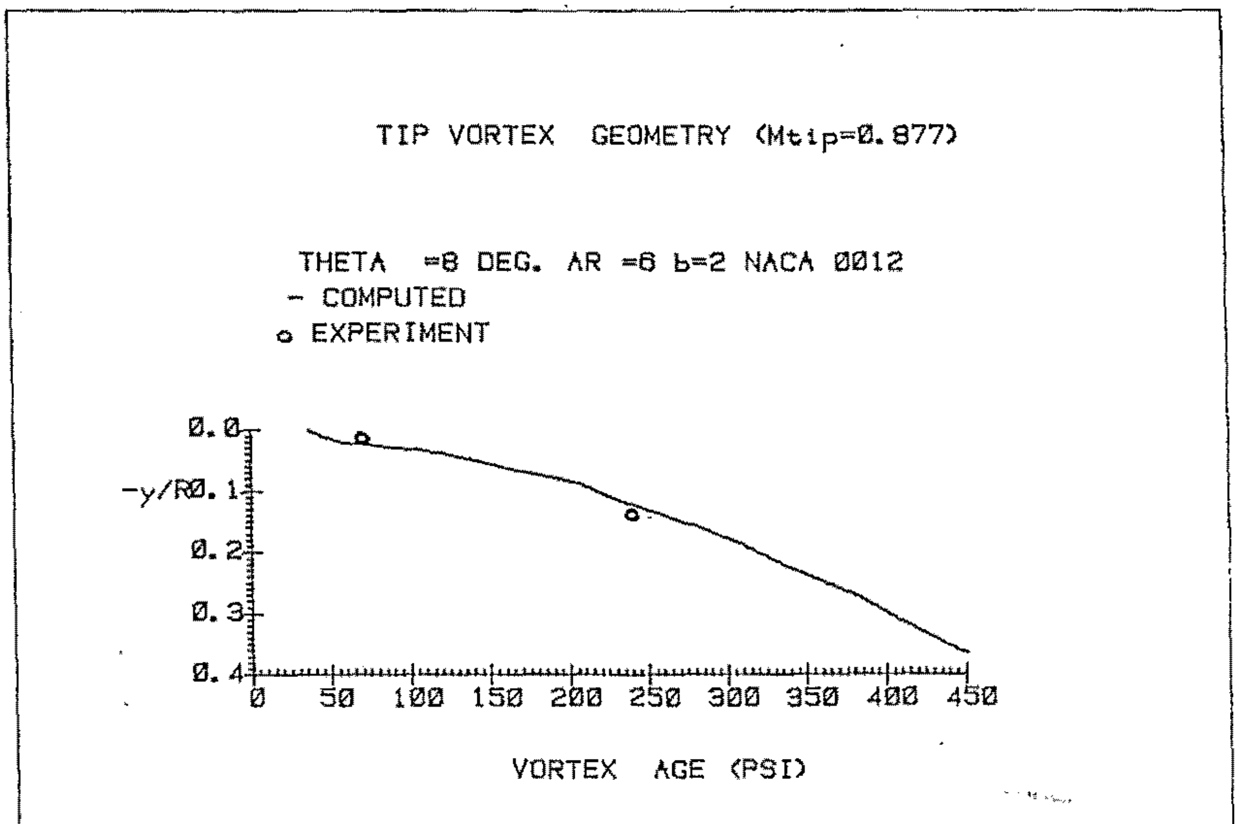

Figure 8.

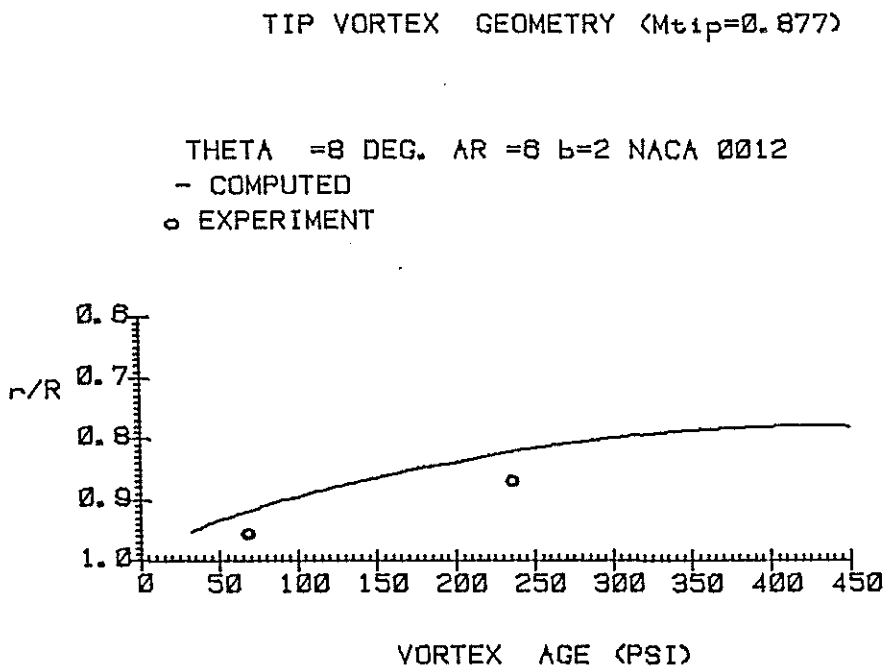

Figure 9.

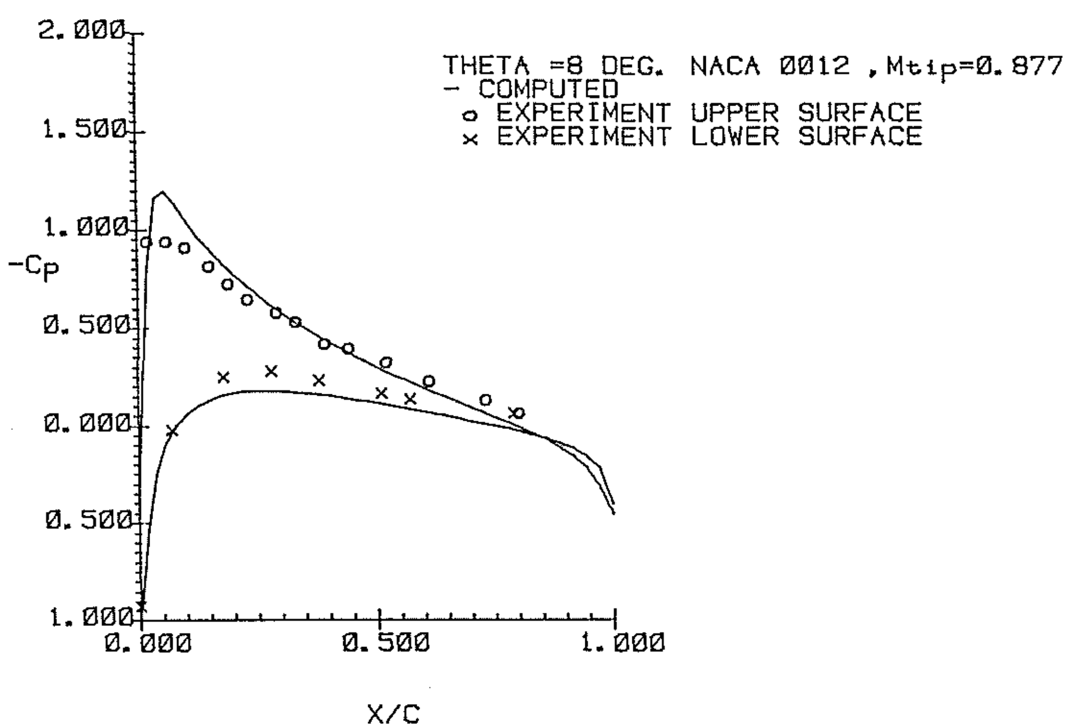

CHORDWISE PRESSURE DISTRIBUTION (AR =6, b =2, r/R=0.68)

Figure 10.

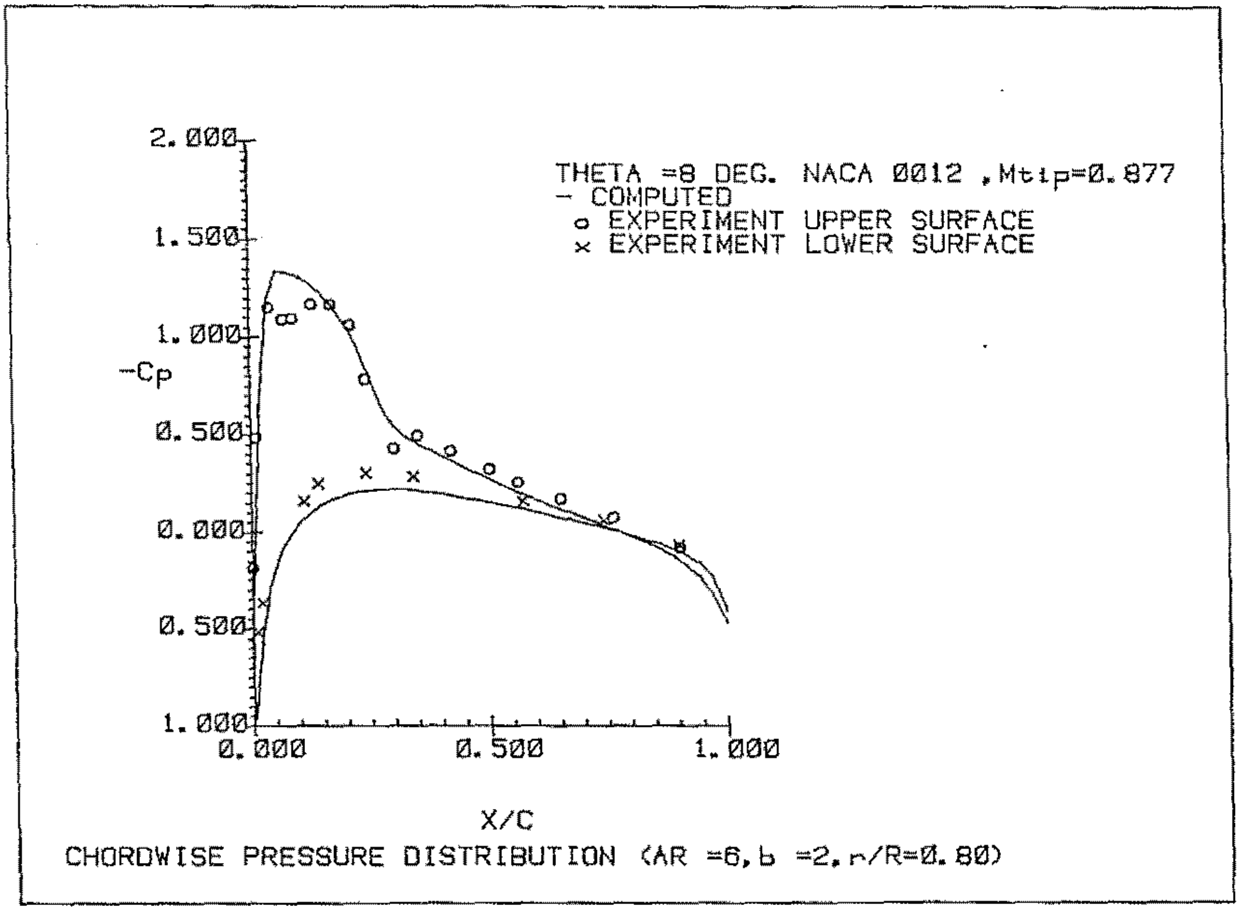

Figure 11.

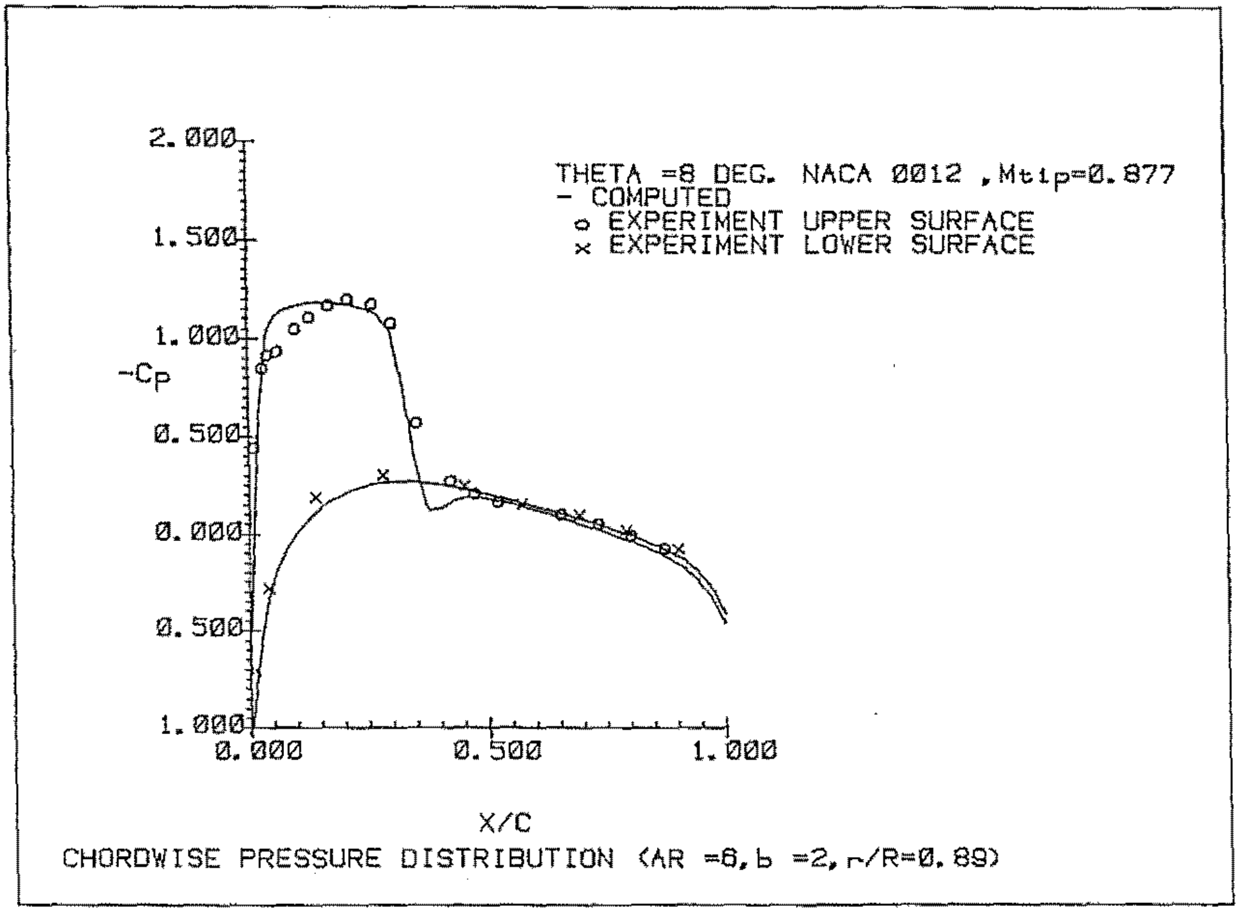

Figure 12.

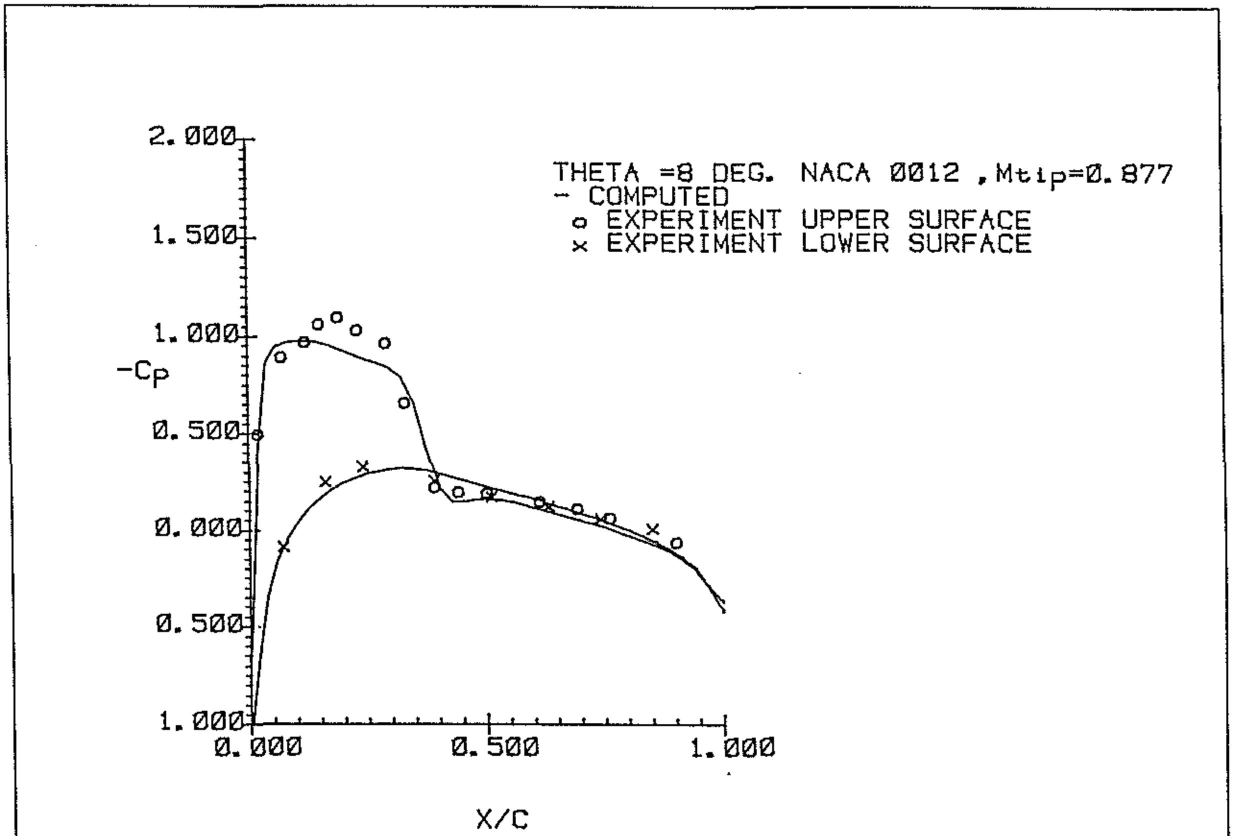

CHORDWISE PRESSURE DISTRIBUTION (AR =6, b =2, r/R=0.96)

Figure 13.

TIP VORTEX COORDINATES (AXIAL)

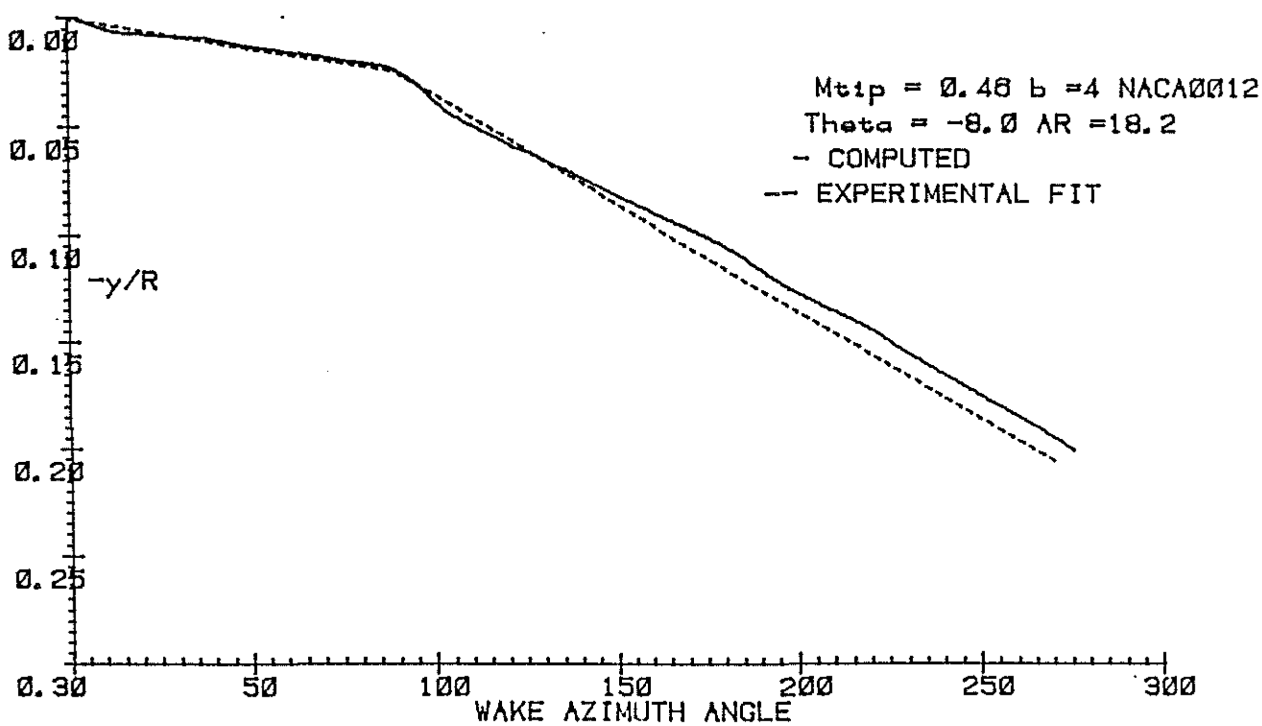

Figure 14.

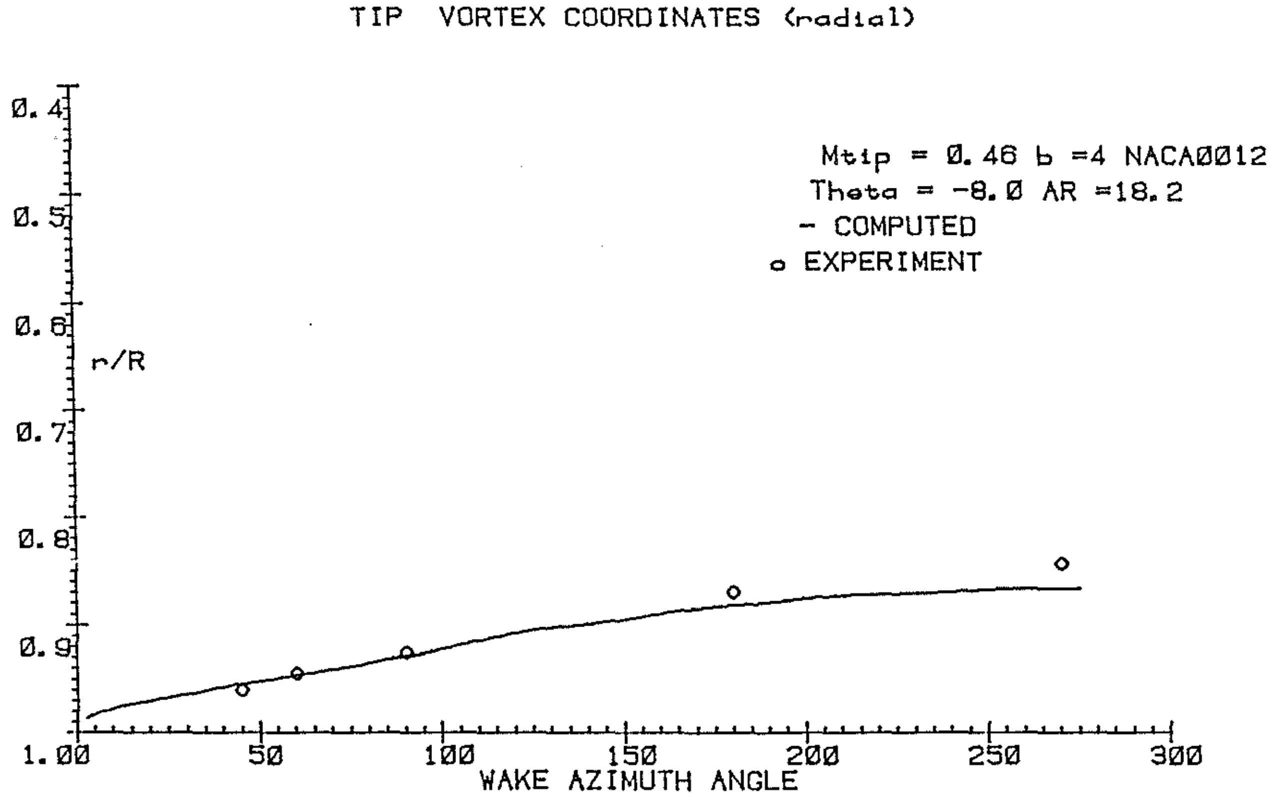

Figure 15.

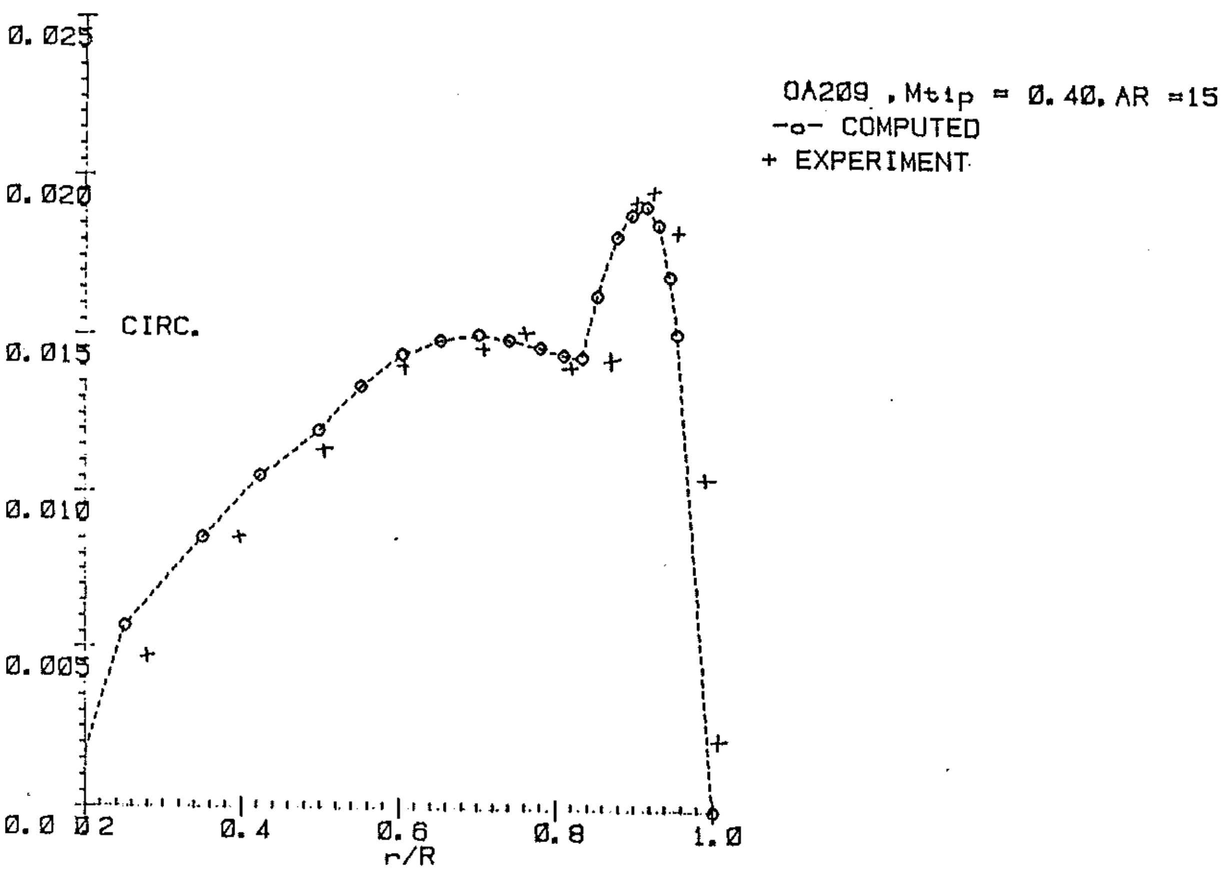

Figure 16.

TIP VORTEX COORDINATES (AXIAL)

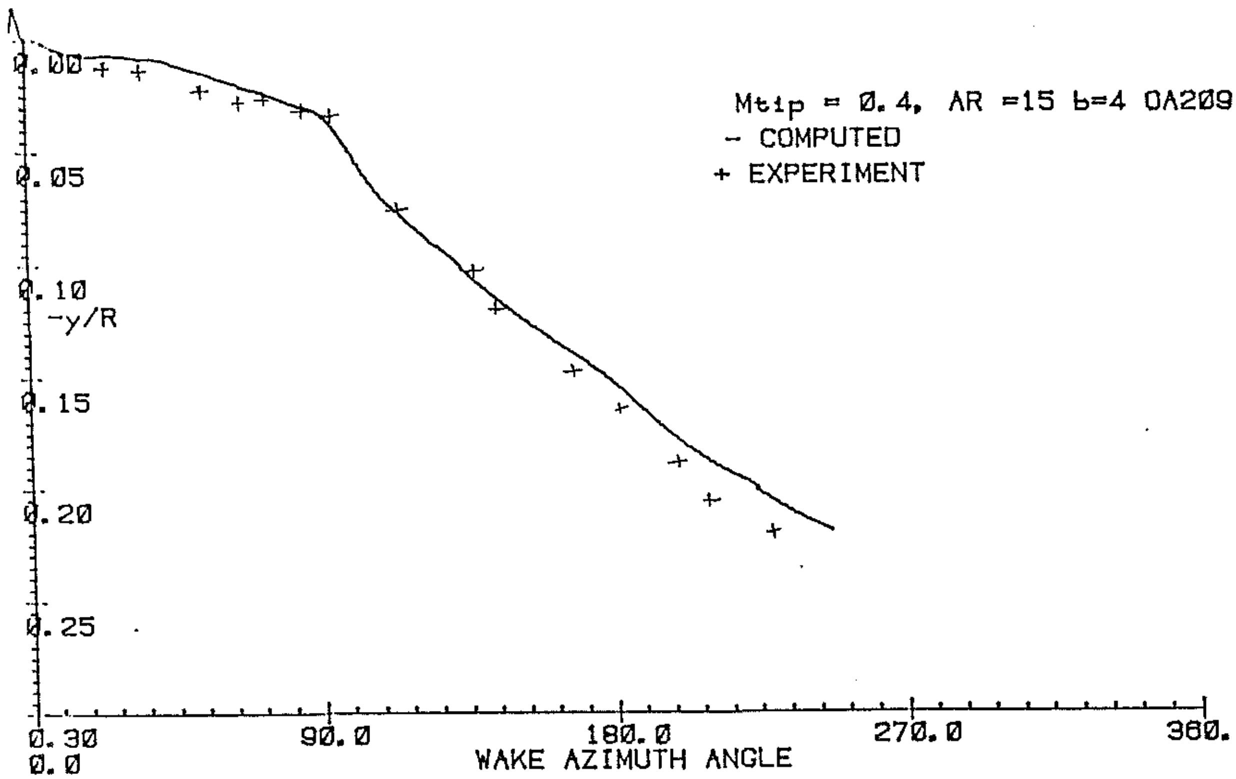

Figure 17.

TIP VORTEX COORDINATES (RADIAL)

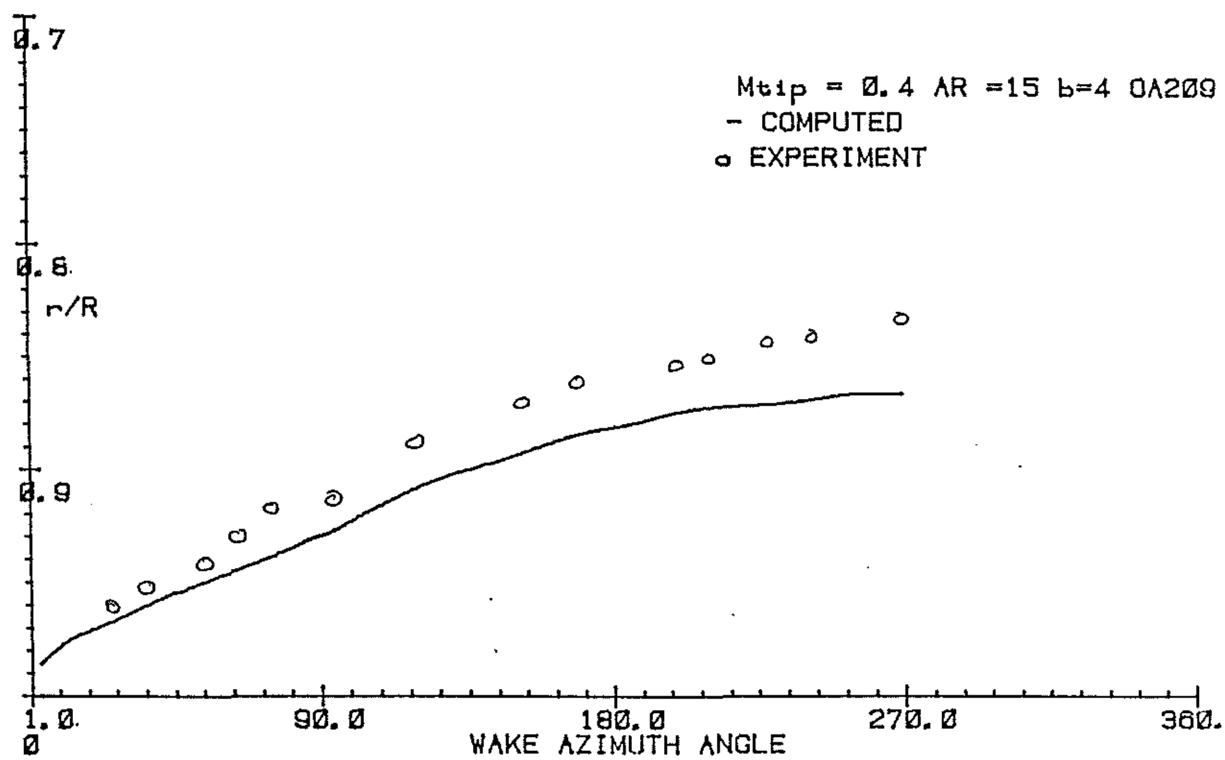

Figure 18.